JGR Atmospheres

RESEARCH ARTICLE
10.1029/2020JD034427

Key Points:

- Simulations by a box model with photochemistry & size-resolved particle microphysics can reproduce the observed evolution of a ship plume
- Significant new particle formation and growth can occur in ship plumes and contribute to ship particle number emissions
- Wind speed, emission rates of SO_2 and NO_x, radiation, temperature, and NH_3 have strong effects on the ship particle number emission index

Correspondence to:
Y. Zhang and F. Yu,
yan_zhang@fudan.edu.cn;
fyu@albany.edu

Citation:
Mao, J., Zhang, Y., Yu, F., Nair, A. A., Yu, Q., Wang, L., et al. (2021). On the ship particle number emission index: Size-resolved microphysics and key controlling parameters. *Journal of Geophysical Research: Atmospheres*, *126*, e2020JD034427. https://doi.org/10.1029/2020JD034427

Received 18 DEC 2020
Accepted 14 JUN 2021

On the Ship Particle Number Emission Index: Size-Resolved Microphysics and Key Controlling Parameters

Jingbo Mao[1,2], Yan Zhang[1,3,4,5], Fangqun Yu[2], Arshad Arjunan Nair[2], Qi Yu[1], Lin Wang[1], Weichun Ma[1], and Limin Chen[1]

[1]Department of Environmental Science and Engineering, Shanghai Key Laboratory of Atmospheric Particle Pollution and Prevention, Fudan University, Shanghai, China, [2]Atmospheric Sciences Research Center, State University of New York, Albany, NY, USA, [3]Big Data Institute for Carbon Emission and Environmental Pollution, Fudan University, Shanghai, China, [4]Institute of Atmospheric Science, Fudan University, Shanghai, China, [5]Shanghai Institute of Eco-Chongming (SIEC), Shanghai, China

Abstract Shipping particle number emission is important as it can influence cloud condensation nuclei abundance and thus indirectly affect clouds and perturb the Earth's radiation budget. Here, we integrate a size-resolved Advanced Particle Microphysics module with a photochemical BOX MOdeling eXtension to the Kinetic PreProcessor and employ the resulting model to understand the microphysical and chemical characteristics of ship plumes. Simulated concentrations of key gaseous species and particle numbers are in good agreement compared with measurements from the NOAA Intercontinental Transport and Chemical Transformation (ITCT) 2K2 field study off the California coast. Further analysis reveals that significant new particle formation can occur in the plume and the growth of these secondary particles to 5–20 nm generally dominates the total particle numbers. We show that wind speed, emission rates of SO_2 and NO_x, solar irradiation, ambient temperature, and background [NH_3] have strong nonlinear effects on the ship particle number emission index (EIPN). Depending on the ambient air and meteorological conditions, the model simulations show that EIPN can range from $\sim 2.5 \times 10^{14}$ no. kg^{-1} fuel (dominated by primary particles) to $\sim 3.0 \times 10^{18}$ no. kg^{-1} fuel (dominated by secondary particles). In consideration of the current worldwide expansion of Emission Control Areas, we systematically study how the EIPN decreases with reduction of fuel sulfur content to 0.1%. Our study highlights the necessity of accounting for the nonlinear dependence of secondary particle formation on key controlling parameters in calculating shipping particle number emissions, which is important for determining aerosol indirect climate effects.

Plain Language Summary Maritime transport emissions are increasing due to increased global trade and as the Arctic Ice fades, fragile pristine environments will increasingly be exposed. Shipping emissions are an important source of tiny atmospheric particles capable of seeding clouds and thus perturbing the Earth's radiation budget. A ship plume, in addition to containing emitted primary particles, is a chemical cocktail capable of forming secondary particles under the right meteorological conditions. Considering the uncertainties in the nonlinear chemical and microphysical processes in ship plumes, we develop a fully solved gas-phase chemistry and size-resolved microphysics model validated by a maritime field campaign. The strong nonlinear effects of wind speed, acidic gas emissions, solar irradiation, ambient temperature, and ammonia on ship-emitted particle numbers are unraveled, showing that the ship particle number emission index can range from $\sim 2.5 \times 10^{14}$ no. kg^{-1} fuel (dominated by primary particles) to $\sim 3.0 \times 10^{18}$ no. kg^{-1} fuel (dominated by secondary particles). Moreover, sulfate aerosols may decrease with the wider application of lower fuel sulfur content regulated by International Marine Organization policies. This study can provide a hitherto missing representation of shipping particle numbers and their nonlinear dependence on key parameters in current numerical models of climate change assessment.

1. Introduction

Shipping emissions have received increasing attention in recent years due to their potential role in air quality, climate change, and human health. Ocean-going ships have emitted 15% of the total global NO_x emissions and 4%–9% of the global SO_2 emissions (Eyring et al., 2010). Ship-emitted NO_x perturbs the $NO_x/HO_x/O_3$

cycles (Lawrence & Crutzen, 1999), and SO_2 contributes to new particle formation and particle growth (Capaldo, Corbett, et al., 1999). In addition to gaseous species, shipping-related particulate matter emissions are responsible for 3%–8% of global $PM_{2.5}$ (Cohen et al., 2005). The various particles emitted by ships, such as black carbon (BC), organic carbon, sulfate, and volatile particles, lead to a complex radiative forcing (Durkee et al., 2000; Jacobson et al., 2011). Ramana and Devi (2016) detected that shipping emissions caused BC concentrations to be enhanced by a factor of four and exerted a strong positive influence on net warming over the southern Bay of Bengal. Christensen et al. (2015) found that the cloud albedo increases five times more in liquid clouds than in mixed-phase clouds in numerous ship tracks. Endresen et al. (2003) estimated the global net radiative forcing from ship emissions using a global Chemical Transport Model (CTM) ranging from 0.01 to 0.02 W m^{-2}. Diamond et al. (2020) calculated the effective radiative forcing from aerosols within the southeast Atlantic shipping corridor as approximately −2 W m^{-2}. Shipping emissions can further affect convection, lightning, and rainfall by influencing the CCN number concentration. Thornton et al. (2017) demonstrated that aerosol particles and NO_x from ships can affect maritime convection and enhance lightning over shipping lanes. Christensen and Stephens (2012) exhibited that drizzle rates along ship tracks decreased (an average relative decrease of 72%) compared to the surrounding clouds by analyzing CloudSat satellite data.

At a given water supersaturation ratio, the number size distribution and composition of atmospheric particles determine the cloud condensation nuclei (CCN) number concentration (Fitzgerald, 1973; Junge & McLaren, 1971). Particles emitted by ships account for a large fraction of global anthropogenic aerosol emissions (Agrawal et al., 2008; Dominguez et al., 2008). Many measurements of the EIPN in fresh ship exhausts have been reported, which are in the range of 0.2–6.2 × 10^{16} no. kg^{-1} fuel (Jonsson et al., 2011; Juwono et al., 2013; Lack et al., 2009, 2011; Sinha et al., 2003; Westerlund et al., 2015). Villa et al. (2019) measured the total EIPN and found an average value of ∼7.6 ± 1.4 × 10^{15} no. kg^{-1} fuel in open waters, while Sinha et al. (2003) reported a value of up to 6.2 ± 0.6 × 10^{16} no. kg^{-1} fuel. Jonsson et al. (2011) showed that EIPN was 2.55 ± 0.11 × 10^{16} no. kg^{-1} fuel at a harbor with numerous ships passing. The soot particle numbers appear to be 1–3 orders of magnitude lower than the total particles, and the majority of which are secondary particles formed in fresh plumes (Lack et al., 2009).

It is imperative to determine the key parameters controlling particle number emissions to better understand the role of ship emissions in terms of CCN abundance over the oceans and coastal areas and their effects on climate change. One key uncertainty in assessing the impact of particles from ships is the nonlinear chemical and microphysical processes in subgrid ship plumes. The evolution of particles in a ship plume has been investigated in several previous studies (Russell et al., 1999; Song, Chen, & Davis, 2003; Tian et al., 2014). Russell et al. (1999) found that the sulfur content of fuel directly influences CCN by using a dynamic box model including nucleation, coagulation, and condensation processes highlighting sulfate, mainly due to SO_2 oxidation, as a key component for new particle formation in ship plumes. Song, Chen, & Davis (2003) studied the sulfur chemistry of ship plumes and noted the importance of photochemistry in the new particle formation rate, but the study could not validate the model predictions due to a lack of observational data from an individual ship plume with specific ship information (e.g., ship type, cruising speed, gross weight, engines, and so on) and meteorological conditions. Tian et al. (2014) applied the Particle Monte Carlo model-Model for Simulating Aerosol Interactions and Chemistry (PartMC-MOSAIC) to explore the evolution of particles in a ship plume and the properties of CCN with the assumption that the initial and background particle size distributions were lognormally distributed. All of these three previous studies applied binary H_2SO_4–H_2O nucleation processes, in which the nucleation rates were estimated based on Kulmala and Laaksonen (1990), Capaldo, Kasibhatla & Pandis (1999), Kuang et al. (2008), respectively. Nevertheless, O'Dowd et al. (1999) speculated that a ternary nucleation mechanism (H_2SO_4–H_2O–NH_3) might be involved in coastal areas. Recent experimental and theoretical studies show that binary H_2SO_4–H_2O nucleation alone cannot account for the new particle formation observed in the boundary layer and that ammonia and ionization play critical roles (Kirkby et al., 2011; Yu et al., 2020; Yu, Nadykto, et al., 2018). In addition, all previous studies on particle formation in ship plumes employed simplified chemistry and aerosol microphysics schemes (to our knowledge).

The main objective of this study is to investigate the key parameters that affect the EIPN using a ship plume box model with fully solved gas-phase chemistry and size-resolved microphysics and employs the ternary

ion-mediated nucleation scheme (Yu et al., 2020; Yu, Nadykto, et al., 2018). The ship plume box model is validated using the quantitative information of a specific ship plume and meteorology from the ITCT 2K2 aircraft campaign (Parrish et al., 2004; Chen et al. (2005), whose measurements have been widely used for studying nonlinear chemistry in ship plumes (e.g., Chen et al., 2005; Kim et al., 2009; Song et al., 2010).

2. Ship Plume Chemistry and the Microphysics Box Model

2.1. BOXMOX

BOX MOdeling eXtension (BOXMOX), an extension to the Kinetic PreProcessor, is a time-varying photochemical box model developed by Ludwig-Maximilians-Universität München, the European Centre for Medium-Range Weather Forecasts (ECMWF) and the National Center for Atmospheric Research (NCAR), which can be applied to chamber experiments, Lagrange-type air parcel studies, and chemistry in the atmospheric boundary layer (https://boxmodeling.meteo.physik.uni-muenchen.de/downloads/boxmox.html, Last access: December 5, 2020). The gas-phase chemical mechanisms in BOXMOX include variants or updated versions of CBM (CB05, CBMZ), RADM (RADM2, RADMK), MCM, RACM, SAPRC99, and MOZART (MOZART-4, MOZART-T1) (Knote et al., 2015), which are typically used in 3-D chemistry transport models (such as WRF-Chem and CMAQ) to describe tropospheric gas-phase chemistry. In this study, we applied the box model to study the evolution of nonlinear chemistry in a ship plume with MOZART-4 mechanism (Emmons et al., 2010), which includes 85 gas species and 196 reactions with all heterogeneous reactions switched off. Nitrous acid (HONO) is known to be an important source of OH radicals (Alicke et al., 2003; Calvert et al., 1994) and is not contained in MOZART-4. We, therefore, added HONO and its related reactions to MOZART-4, as listed below, with some of the most critical O_3–NO_x–OH reactions. In the present study, the photolysis rates are set as constants based on the values from the fight measurements, mainly including j(NO_2) and j($O(^1D)$).

$$HONO + h\nu \rightarrow OH + NO \quad (1)$$

$$OH + NO \rightarrow HONO \quad (2)$$

$$OH + HONO \rightarrow NO_2 + H_2O \quad (3)$$

$$NO + NO_2 + H_2O \rightarrow 2HONO \quad (4)$$

$$NO + O_3 \rightarrow NO_2 + O_2 \quad (5)$$

$$NO_2 + h\nu \rightarrow O\left(^3P\right) + NO \quad (6)$$

$$O\left(^3P\right) + O_2 \xrightarrow{m} O_3 \quad (7)$$

$$O_3 + h\nu \rightarrow O\left(^1D\right) + O_2 \quad (8)$$

$$O\left(^1D\right) + H_2O \rightarrow 2OH \quad (9)$$

2.2. Advanced Particle Microphysics (APM) Model

The Advanced Particle Microphysics (APM) model, a multi-type, multi-component, size-resolved box model, is the result of past development and validation efforts aimed at explaining atmospheric particle observations (e.g., Luo & Yu, 2011; Turco et al., 1979; Yu, 1998; 2006; Yu & Luo, 2009; Yu & Turco, 1997). Microphysical processes include nucleation, condensation/evaporation, coagulation, and thermodynamic equilibrium, with local humidity and without considering dilution in the APM model. Yu (2010) employed

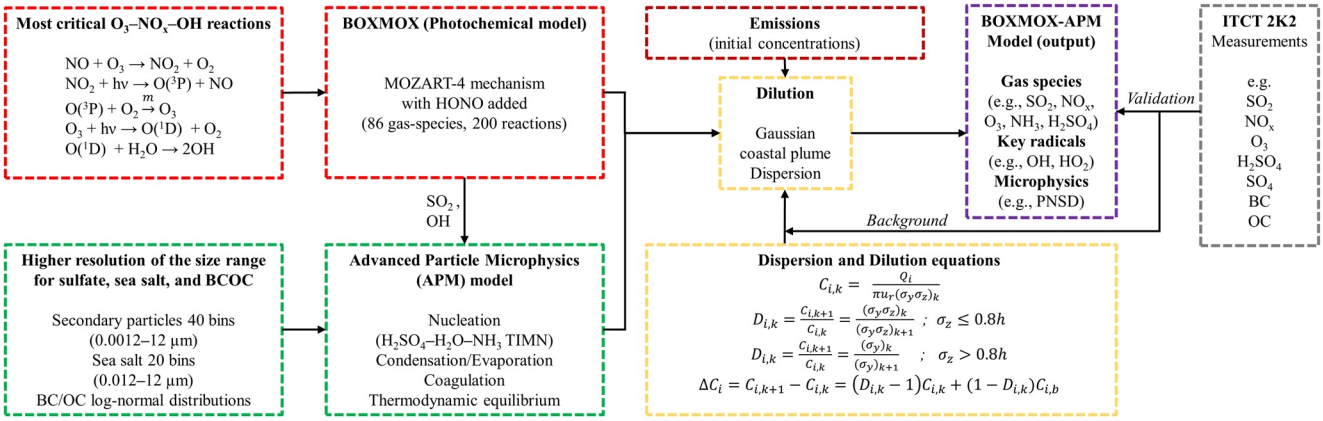

Figure 1. Flowchart of BOXMOX-APM.

this microphysical box model to successfully reproduce the number concentrations of ultrafine particles in SO_2 plumes emitted from a smelter, which were consistent with the observations. To study the nucleation process, we employ an up-to-date version of H_2SO_4–H_2O–NH_3 ternary ion-mediated nucleation (TIMN) scheme developed by Yu et al. (2020), Yu, Nadykto, et al. (2018). The six key parameters controlling the new particle formation rates in TIMN are: gaseous sulfuric acid concentration ([H_2SO_4]), temperature (T), relative humidity (RH), ionization rate (Q), surface area of background particles (SB), and ammonia concentration ([NH_3]).

2.3. Ship Plume Model–BOXMOX–APM

To investigate the full chemical evolution of gas phases and size-resolved particle microphysics in a ship plume, we coupled BOXMOX with APM, and the flowchart of the BOXMOX-APM box model is shown in Figure 1. We assumed that the ship exhaust is not further influenced by emissions after it leaves the funnel. The plume gets diluted, and the cross section of the plume increases. The model simulates gas and particle concentrations as the plume exhaust evolves and treats the mixing of the plume with background air.

For the dilution process in the BOXMOX-APM model, we apply a Gaussian plume dispersion originally developed by Hanna et al. (1985) and further adapted by Song, Chen, Hanna, et al. (2003) and Kim et al. (2009). The plume concentration of species i at the time steps k and k+1 ($C_{i,k}$ and $C_{i,k+1}$, g m^{-3}) can be calculated as:

$$C_{i,k} = \frac{Q_i}{\pi u_r \left(\sigma_y \sigma_z\right)_k} \tag{10}$$

$$C_{i,k+1} = \frac{Q_i}{\pi u_r \left(\sigma_y \sigma_z\right)_{k+1}} \tag{11}$$

where Q_i is the emission rate (g s^{-1}) of species i from the ship plume, u_r is the wind speed (m s^{-1}), and σ_y and σ_z represent the lateral and vertical turbulent dispersion parameters (m), respectively. Kim et al. (2009) derived detailed formulas for σ_y and σ_z on the basis of the downwind distance $\left(x\left(m\right)\right)$ and Pasquill stability class, including very unstable (class A), unstable (class B), slightly unstable (class C), neutral (class D), slightly stable (class E), and stable (class F). We applied these formulas (as given in Table 1 of Kim et al., 2009) to calculate σ_y and σ_z in the present study.

The dilution factors for species i ($D_{i,k}$) are expressed as the following equations (Kim et al., 2009; Song, Chen, & Davis, 2003):

$$D_{i,k} = \frac{C_{i,k+1}}{C_{i,k}} = \frac{\left(\sigma_y \sigma_z\right)_k}{\left(\sigma_y \sigma_z\right)_{k+1}}, \quad \sigma_z \le 0.8h \tag{12}$$

$$D_{i,k} = \frac{C_{i,k+1}}{C_{i,k}} = \frac{\left(\sigma_y\right)_k}{\left(\sigma_y\right)_{k+1}}, \quad \sigma_z > 0.8h \tag{13}$$

where h is the mixing layer height (m). The change in the concentration of species i (ΔC_i) in the plume through mixing with its background concentration $C_{i,b}$ (g m^{-3}) can be written as:

$$\Delta C_i = C_{i,k+1} - C_{i,k} = \left(D_{i,k} - 1\right)C_{i,k} + \left(1 - D_{i,k}\right)C_{i,b} \tag{14}$$

3. Comparison of BOXMOX-APM Simulations With ITCT 2K2 Measurements

3.1. Model Setup

For a case study using the BOXMOX-APM model, we chose measurements from the ITCT 2K2 airborne field campaign conducted at ~11 a.m. on May 8, 2002 by the NOAA WP-3D aircraft (Chen et al., 2005). The observed ship was identified as a bulk carrier running on marine fuel oil, whose fuel combustion rate was 27 tons per day and engine load was 67% (Chen et al., 2005). The gas-phase species (e.g., NO_x, SO_2, H_2SO_4, O_3, and NMVOCs), particle numbers, and meteorological conditions were measured in eight transects along the ship plume, with the exhaust plume age ranging from ~0.5 to 3 h. Detailed information on data and sampling instruments has been summarized in previous literatures (Brock et al., 2004; Chen et al., 2005; Nowak et al., 2004; Parrish et al., 2004). For meteorological conditions, sky conditions, stability class, wind speed, and wind direction are based on Chen et al. (2005); mixing heights are derived from the study of Kim et al. (2009); pressure, temperature, relative humidity (RH), j(O^1D), and j(NO_2) are calculated based on the ITCT 2K2 airborne field campaign. The emission rates of NO_x and SO_2 are derived from Chen et al. (2005), who evaluated their emission rates based on the mass ratio of CO_2 using the data from The ITCT 2K2 ship plume experiment. NMVOCs (ethane, ethene, formaldehyde, and benzene) are considered in the present study, with their emission rates based on the results of Song et al. (2010) and their background concentrations from the ITCT 2K2 flight campaign. The emission factors of particle components (SO_4^{2-}, BC, and OC) are based on the TexAQS/GoMACCS 2006 field study, which was carried out from Charleston, South Carolina to Houston, Texas, with most sampling occurring in the Gulf of Mexico, Galveston Bay, and the Houston Ship Channel (Lack et al., 2009), due to the lack of emission information of the particle compositions in the ITCT 2K2 observations. The emission factor of NH_3, a key parameter impacting new particle formation, is 0.003 g kWh^{-1} (Cooper & Gustafsson, 2004). In our box model with a Gaussian dispersion, the emissions of pollutants are converted into initial concentrations calculated using Equation 10. The background concentrations (except for NH_3) are obtained from the ITCT 2K2 flight campaign. The background concentration of NH_3 is assumed to be 1 ppbv based on GEOS-Chem simulations in the area where ITCT 2K2 measurements were collected (Yu, Nair, & Luo, 2018). Table 1 summarizes the simulation conditions used in the present study.

3.2. Measurements Versus Model Simulations

The measurements took place at approximately 11 am local time around 100 km off the coast of California (Chen et al., 2005). Figures 2 and 3 show the model-simulated changes in the major trace gas species concentrations (SO_2, NO_x, O_3, OH, H_2SO_4, and NH_3) and total particle number concentrations as the ship plume evolved and aged up to 3 h after emission. As a result of dilution and chemical reactions, the primary pollutants NO_x and SO_2 decrease rapidly, and both drop quickly below 10 ppbv within 10–15 min after emission (Figures 2a and 2b). As shown in Figure 2c, O_3 is titrated because of the high levels of NO via reaction 5 during the early plume development stage, as we applied a NO:NO_2 ratio of 96:4 reported by the EPA (2000), and then is recovered via the reaction of O_2 and increasing O(^{3}P) generated by the photolysis

Table 1
Simulation Conditions Used in the Present Study for ITCT 2K2 Ship Plume Case Study

Variables	Values
Emission rates (g s^{-1})	
NO_x	6.25
SO_2	9.38
CO	0.74375
NH_3	0.0055
HCHO	0.04
C_2H_4	0.043
C_2H_6	0.001
C_6H_6	0.108
SO_4	0.247
BC	0.119
OC	0.594
Ship information	
Moving direction	WNW
Speed (knot)	9.7
Meteorological conditions	
Sky condition	Clear sky
Stability class	Neutral stable (D)
Wind velocity (m s^{-1})	9–11
Wind direction	SSE
Mixing height (m)	800
Pressure (hPa)	1002
Temperature (K)	283
RH (%)	88
$j(O^1D)$ (s^{-1})	3.79×10^{-5}
$j(NO_2)$ (s^{-1})	7.80×10^{-3}
Aerosol-related variables	
XQ (ion pairs cm^{-3} s^{-1})	5
Background gas concentrations (ppbv)	
[NO_x]	0.14
[O_3]	40
[CO]	130
[SO_2]	0.4
[NH_3]	1
[C_3H_8]	0.37
[H_2SO_4]	0.0004
[PAN]	0.135
Background particle concentrations (μg m^{-3})	
[SO_4]	1
[BC]	5
[OC]	2
[SEA SALT]	30

of NO_2 (reactions 6 and 7) as the NO_x concentration decreases. The simulated concentrations of SO_2 and NO_x are slightly lower than the observations with NMBs (normalized mean biases) of −7.03% and −28.04%, while the calculated O_3 is in good agreement with the observations (NMB = −1.59%). Overall, the model captures the changes of major species in the ship plume. For OH radicals, the peak value is similar to the results of Chen et al. (2005) and Kim et al. (2009), reaching ~1.52×10^7 no. cm^{-3} at ~57 min after the ship exhaust was emitted (Figure 2d). Photolysis of O_3 is the predominant source of OH radicals via reactions 8 and 9. As discussed above, O_3 is depleted and is low in concentration during the early plume stage, causing low production of OH. Thereafter, OH radicals increase following the recovery of O_3. The uncertainties in simulating SO_2, NOx, and O_3 by the box model may be caused by, but not limited to, chemical mechanism, microphysical conditions, and dilution process.

Figure 3a shows a comparison of BOXMOX-APM-simulated gaseous H_2SO_4 concentration ([H_2SO_4]), which is critical for secondary particle formation and growth in ship plumes, with the observations and those predicted by Chen et al. (2005) and Kim et al. (2009). Chen et al. (2005) underestimated H_2SO_4 by a factor of two compared with observations due to OH being underpredicted by a factor of two. The simulated [H_2SO_4] in the present study is higher than that from Kim et al. (2009). While the modeled [H_2SO_4] is higher than that observed in the young ship plume (time (t) < ~70 min), it agrees reasonably well with the measured values when the plume age is >~70 min. The production of H_2SO_4 is controlled by the reaction of SO_2 with OH, while the condensation sink (CS) depends on the surface area of pre-existing particles. The CS is controlled by background aerosols and does not change considerably after t > ~10 min (Figure 3b), and thus it is unlikely to be the source of large differences in [H_2SO_4] at a young plume age. Since the predicted [SO_2] is close to the measurements (Figure 2a), the large discrepancies between the observed and simulated [H_2SO_4] when the plume age is <~70 min may be caused by the possible overestimation of OH radicals. On the other hand, [H_2SO_4] was measured with a chemical ionization mass spectrometer (CIMS) during ITCT 2K2 (Chen et al., 2005), and it is well recognized that the CIMS [H_2SO_4] measurements are likely to have large uncertainties due to the uncertainty in the charge efficiency, calibration errors, and formation of sulfuric acid clusters (a factor of two or more, Neitola et al., 2015), especially in the plumes with the airborne approach. Further investigation is needed to resolve this difference. Figure 3b shows that ship-emitted NH_3 gets quickly mixed with ambient air within ~5 min and that the ambient level of NH_3 affects the nucleation rate. Figure 3c shows the evolution of primary, secondary, and total particle numbers with diameters larger than 5 nm, which indicates that the total particle numbers (>5 nm) are consistent with observations with NMB of 9.49% and are dominated by secondary particles. The total particle numbers rapidly decreased in the fresh plume owing to dilution, then increased, and finally, slowly decreased as a result of nucleation, growth, and coagulation. The primary (or pre-existing) particle number concentrations decreased quickly and approached the background level because of the dilution process. Additionally, the simulated particle number concentration

Table 1
Continued

Variables	Values
[DUST]	1

is lower than the observed value when the plume age is ~40 min, although overpredicted [H_2SO_4] (Figure 3a) would lead to high nucleation and growth rates at that time. This underestimation could be associated with an under-predicted growth rate, possibly due to other species, since [H_2SO_4] was already over predicted. The underprediction of growth could also be caused by the biogenic VOCs from the marine surface (Arnold et al., 2009; Griffin et al., 1999; Gantt et al., 2010; Hoffmann et al., 1997), which are not considered in this study. Overall, the results indicate that the ternary ion-mediated nucleation (TIMN) scheme is reasonable to investigate the microphysical evolution of aerosol particles in ship plumes in the marine boundary layer.

Figure 3d shows the evolution of the secondary particle number size distributions as the plume aged. New particle formation occurred at ~20 min of the plume age, and then a large fraction of these new particles grew further to 5–20 nm. Under the conditions of the ITCT 2K2 case study, secondary particles dominate the total particle number concentrations in the ship plume.

4. Key Parameters Controlling the Ship Particle Number Emission Index

The formation of secondary particles, which generally dominate the particle number in the ship plume, depends on the gaseous H_2SO_4 and ammonia concentrations, temperature, and pre-existing particles. By affecting H_2SO_4 production in the ship plume, SO_2 and OH radicals also influence ship particle number emission, and OH radicals are further controlled by the nonlinear chemistry of $NO_x/HO_x/O_3$. Therefore, it is necessary to systematically investigate the sensitivity of the ship particle number emission index to key parameters, including stability class, wind speed, sea salt, photolysis rates of NO_2 and $O(^1D)$ (cloudy and clear sky conditions, and solar radiation), ambient temperature, emission rates of SO_2 and NO_x, and background [SO_2], [NO_x], [O_3], and [NH_3]. In the present sensitivity study, the ranges of wind speed, ambient [NO_x] and [O_3] are 2–20 m s^{-1}, 10–6,000 pptv, and 5–75 ppbv, respectively (Vinken et al., 2011); and temperature varies from 250 to 310 K (Fagerlund et al., 2019; Yang et al., 2015). Vinken et al. (2011) determined emission rates of NO_x in the range of 4–184 g s^{-1}, and Diesch et al. (2013) calculated NO_x emission rate at 2.4 g s^{-1}, so we tested NO_x emission rates ranging widely from 0.5 to 190 g s^{-1}. Song, Chen, & Davis (2003) chose SO_2 emission rates ranging from 13 to 90 g s^{-1}, and Cao et al. (2019) detected SO_2 emission rates varying from 0.01 to 0.02 g s^{-1} in the inland waterway of the Jiangsu province, so we used SO_2 emission rates in the wide range of 0–90 g s^{-1}. We applied ambient [SO_2] varying from 0.5 to 15 ppbv, as its background concentration can reach up to ~14 ppbv in the Shanghai port (X. Wang et al., 2019). Quinn et al. (1987) reported [NH_3] in marine air in the range of 0.01–10 ppbv.

The emission index of particle number (EIPN) can be calculated as:

$$\mathrm{EIPN} = \frac{\left(\left[PN_{tot}\right] - \left[PN_{bg}\right]\right) \times 10^6 \times u_r \times S}{CRFUEL} \tag{15}$$

where the unit of EIPN is no. kg^{-1} fuel; $[PN_{tot}]$ and $[PN_{bg}]$ represent the total and background particle number concentrations, respectively, and both units are no. cm^{-3}; and u_r, S, and $CRFUEL$ represent the resulting wind speed, sectional area, and fuel combustion rate, whose units are m s^{-1}, m^2, and kg fuel s^{-1}, respectively. Because of new particle formation and growth, the EIPN changes with plume age. In this study, we use the EIPN at the plume age of 2 h to represent relatively well-developed and aged ship plumes.

For the sensitivity studies presented below, we varied the values of one selected parameter with all other parameters, which are the same as those for the ITCT 2K2 case study described in Section 3.

4.1. Stability Class, Wind Speed, and Background Sea Salt Particles

The SO_2 and OH concentrations are largely controlled by dilution factors that depend on stability classes. Figure 4a shows the emission index of the total, secondary, and primary particle numbers ($EIPN_{TP}$, $EIPN_{SP}$, and $EIPN_{PP}$), plume cross-sectional area (S), N_{SP} $\left(\left[PN_{tot}\right] - \left[PN_{bg}\right]\right)$, and two-hour averaged nucleation

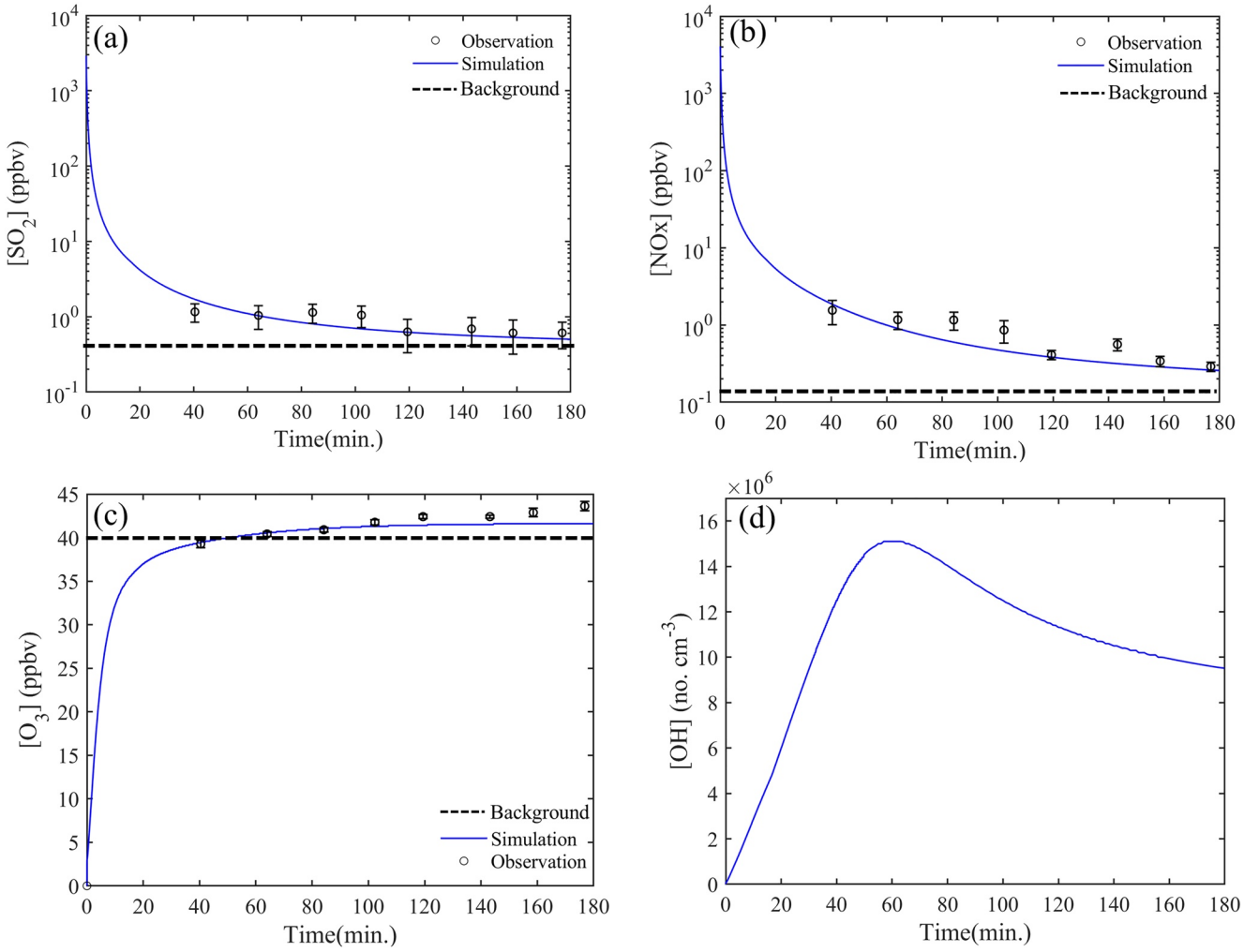

Figure 2. Changes of gaseous species' concentrations along the ship-plume travel times in the ship plume: (a) SO_2, (b) NO_x, (c) O_3, and (d) OH. The solid line represents simulations, circles represent observed mean concentrations, and the dashed line represents average background concentrations.

rate as a function of the stability class. Not surprisingly, $EIPN_{TP}$ is strongly sensitive to the stability class when $EIPN_{SP}$ dominates, decreasing from extremely unstable (class A) to stable (class E) atmospheric conditions. The $EIPN_{SP}$ level is higher under unstable conditions, which is caused by quick dilution and a larger cross-sectional area, although there is less new particle formation per unit area (see the nucleation rate and newly formed secondary particle concentration in Figure 4a. Under real marine boundary layer (MBL) conditions, the most common stability condition to occur over the open ocean is "neutral", and the "unstable" condition is a relatively unlikely setting (Song, Chen, Hanna, et al., 2003). The "stable" class may also occur over the open ocean under certain circumstances (Frick & Hoppel, 2000). The ITCT 2K2 measurements used in the present study were measured under clear-sky neutral condition (Chen et al., 2005). We were not able to find other suitable datasets under a wider range of meteorological conditions that can be used to constrain the model study.

Wind speed, a key parameter of the dilution factor, can affect the EIPN via the dilution process. As "neutral" is the most common stability class in the MBL, we test the sensitivity of wind speed under neutral conditions. Meanwhile, sea salt is generally the dominant background aerosol mass in the marine environment. There is a strong functional relationship between the sea salt aerosol concentration and surface wind speed, as shown by the following formula: $C_{sea-salt} = Aexp(b \cdot u_{10})$, where parameters A and b are set as 3.33 μg m^{-3} and 0.24 s m^{-1}, respectively (Gong et al., 1997). Figure 4b gives $EIPN_{TP}$, $EIPN_{SP}$, $EIPN_{PP}$, N_{SP}, total condensation sink (CS), and two-hour averaged nucleation rate (J) as a function of wind speed. Figure 4b shows

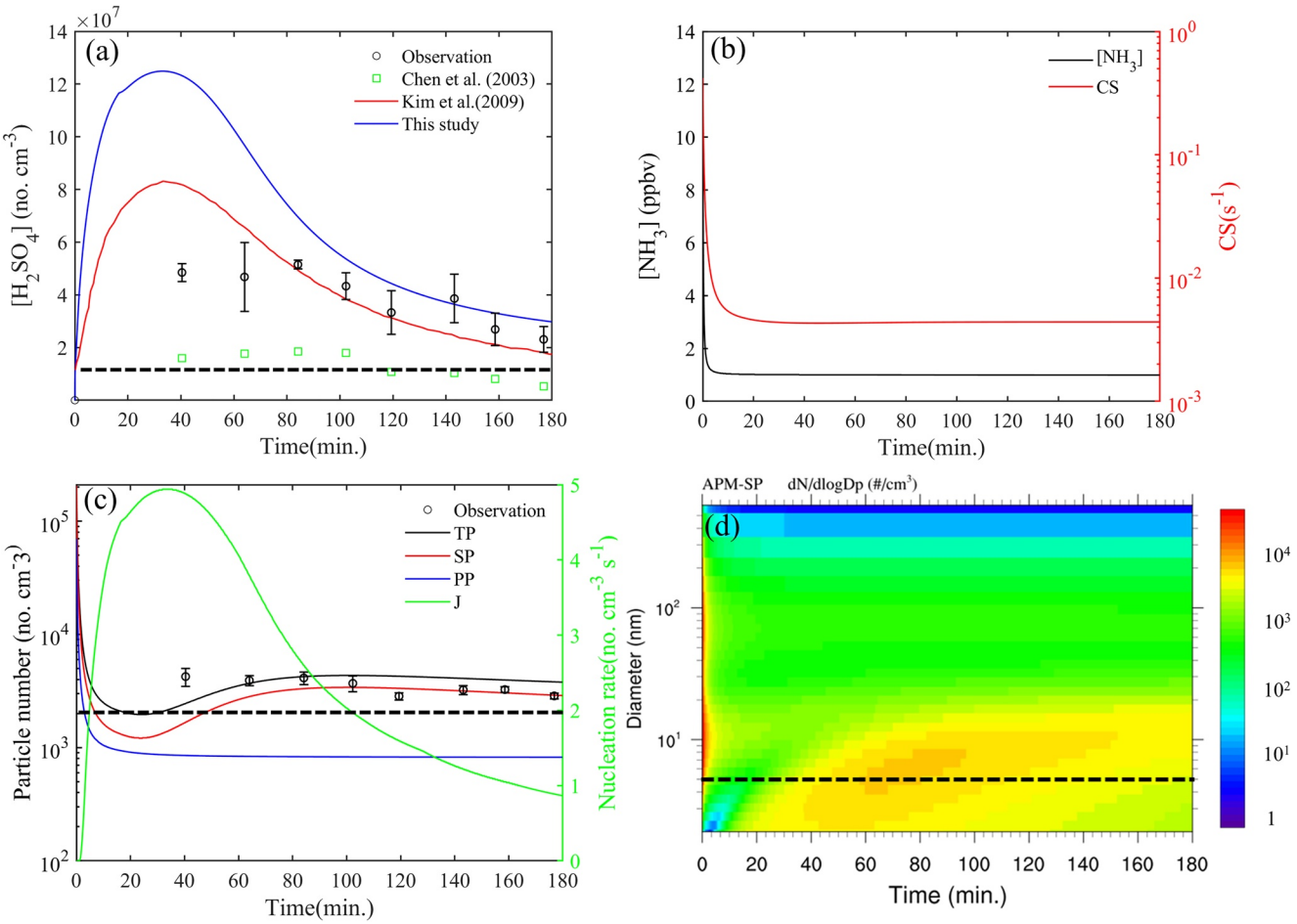

Figure 3. Changes of parameters related to particle numbers with respect to the ship-plume travel time: (a) H_2SO_4, (b) NH_3 and condensation sink (CS), (c) particle number concentrations (TP, SP, and PP represent total, secondary, and primary particle number, respectively) with diameter over 5 nm and nucleation rate (J), (d) simulated evolution of particle number size distributions. The solid lines represent simulations, and circles represent observed mean concentrations in (a and c). The squares in (a) are simulated [H_2SO_4] by Chen et al. (2005). The dashed line in (d) marks 5 nm diameter.

that $EIPN_{SP}$ ranges from 1.0×10^{14} to 1.01×10^{17} no. kg^{-1} fuel, with a three orders of magnitude difference, while $EIPN_{PP}$ is at a constant value of $\sim 2.50 \times 10^{14}$ no. kg^{-1} fuel (as expected). $EIPN_{SP}$ is very sensitive to wind speed, a 1 m s^{-1} difference, with wind speed increasing from 15 to 16 m s^{-1}, can cause up to one order of magnitude change in the nucleation rate, N_{SP}, and $EIPN_{SP}$. At a wind speed of 2 m s^{-1}, large accumulation of ship-emitted BC and OC and the small cross-sectional area caused by a low dispersion rate lead to $EIPN_{SP}$ value below 10^{15} no. kg^{-1} fuel. Also, the sea salt concentration increases with increasing wind speed, leading to H_2SO_4 and small clusters scavenged by abundant pre-existing particles (sea salt) and further affecting nucleation, N_{SP}, and $EIPN_{SP}$. Under the specified conditions, new particle formation is negligible when wind speed is over 16 m s^{-1}, mainly due to the scavenging by sea salt particles in the ship plume. The impact of sea salt emissions on new particle formation in ship plumes and in the marine boundary layer may have important implications for potential climate interventions, such as marine cloud brightening, which can be a subject of future research.

4.2. Photolysis

To study the impact of photolysis, we chose the sunlight intensity of one day (the variable SUN in the BOX-MOX model) as an index to represent photolysis, and only the associated $j(NO_2)$ and $j(O(^1D))$ changes are taken into consideration. The dependence of $EIPN_{TP}$, $EIPN_{SP}$, $EIPN_{PP}$, and two-hour averaged [OH] radicals on the ship exhaust release time varying from 00:00 to 21:00 local time, with the other parameters set the

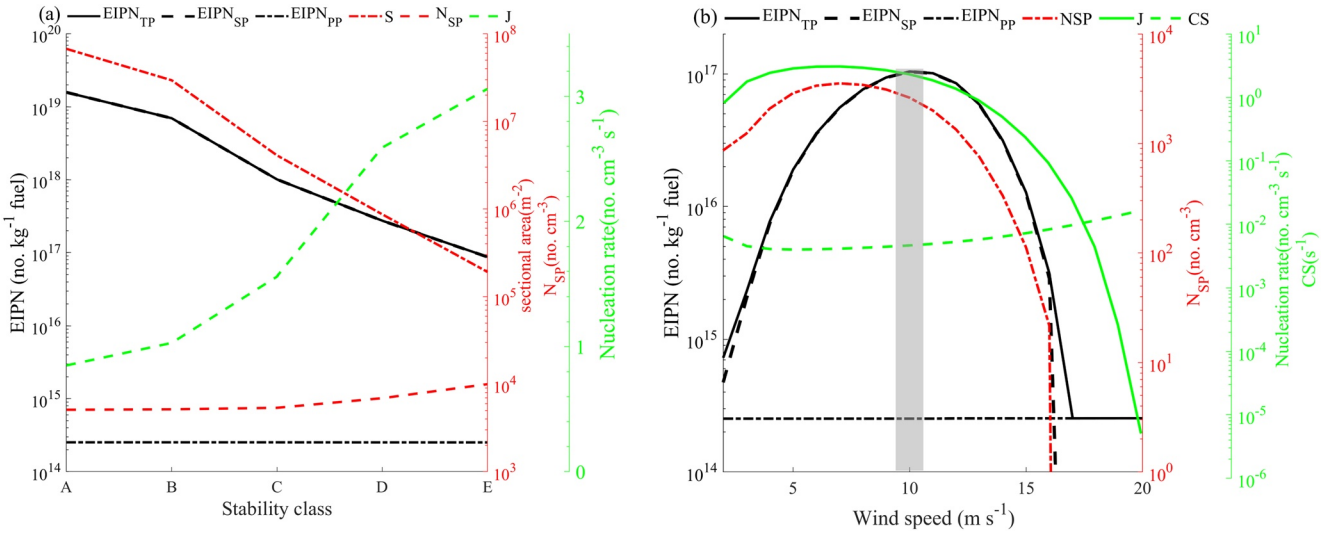

Figure 4. (a) Emission index of total, secondary, and primary particle numbers ($EIPN_{TP}$, $EIPN_{SP}$, $EIPN_{PP}$), sectional area of plume (S), N_{SP} ([PN_{tot}]-[PN_{bg}]), and two-hour averaged nucleation rate (J) as a function of stability class; (b) Emission index of total, secondary, and primary particle numbers ($EIPN_{TP}$, $EIPN_{SP}$, $EIPN_{PP}$), condense sink (CS), N_{SP} ([PN_{tot}]-[PN_{bg}]), and two-hour averaged nucleation rate (J) as a function of wind speed. The range of wind speed measured during the ITCT 2K2 experiment is shaded in gray.

same as in the baseline case, is shown in Figure 5a. As expected, $EIPN_{SP}$ is sensitive to the sunlight intensity during the daytime, with the value of $EIPN_{SP}$ varies from 3.40×10^{14} to 1.27×10^{17} no. kg^{-1} fuel. When the release of the ship plume occurs during morning and night hours, OH radical levels are too low to oxidize SO_2 in the plume to nucleate new particles.

Clouds affect the sunlight intensity; Figure 5b compares $EIPN_{SP}$ under a clear sky and a cloudy sky at two different temperatures (260 and 300 K). The cloud optical depth is set to 37.3 in the present study (Hong et al., 2007). Not surprisingly, it is favorable for new particle formation during the daytime under a clear sky condition. Cloudy conditions can reduce photolysis rates, which can decrease the production of OH radicals and result in 1–2 orders of magnitude decrease in $EIPN_{SP}$ compared to that under clear sky conditions.

The sunlight intensity can change with latitude, solar zenith angle, cloud cover, aerosols, etc. Hence, it is convenient to relate solar irradiation (G) to the photolysis rates of NO_2 and $O(^1D)$, following the formulas reported by Trebs et al. (2009) and Palancar et al. (2005), respectively:

$$j\left(NO_2\right) = \left(1 + 0.04\right) \times \left(1.47 \times 10^{-5} \times G - 4.84 \times 10^{-9} \times G^2\right) \quad (16)$$

$$j\left(O(^1D)\right) = 1.9 \times 10^{-5} \times G_{UV-B} + 1.46 \times 10^{-6} \quad (17)$$

Figure 5c shows $EIPN_{TP}$, $EIPN_{SP}$, $EIPN_{PP}$, N_{SP}, two-hour averaged nucleation rate (J), and two-hour averaged [H_2SO_4] as functions of solar irradiation. Solar radiation has a strong nonlinear effect on $EIPN_{SP}$, increasing from lower than 1.0×10^{14} (no nucleation occurred) to 1.56×10^{17} no. kg^{-1} fuel as G increases from near zero to 1200 W m^{-2}. Not surprisingly, low solar irradiation, for example during the night, morning, or on a cloudy day, leads to low photolysis rates, which results in low OH radical concentrations, [H_2SO_4], nucleation rate, and N_{SP} in the ship plume.

4.3. Temperature

Figure 6 illustrates that the dependence of $EIPN_{TP}$, $EIPN_{SP}$, $EIPN_{PP}$, two-hour averaged nucleation rate, and N_{SP} on temperature (T). Temperature has an intense impact on $EIPN_{SP}$, which varies from 1.23×10^{15} to 3.81×10^{18} no. kg^{-1} fuel. $EIPN_{SP}$ is insensitive to T when T changes from 270 to 280 K (0.05 no. cm^{-3} s^{-1}<nucleation rate<0.1 no. cm^{-3} s^{-1}) and from 300 to 310 K (nucleation rate<0.0001 no. cm^{-3} s^{-1}) but is very sen-

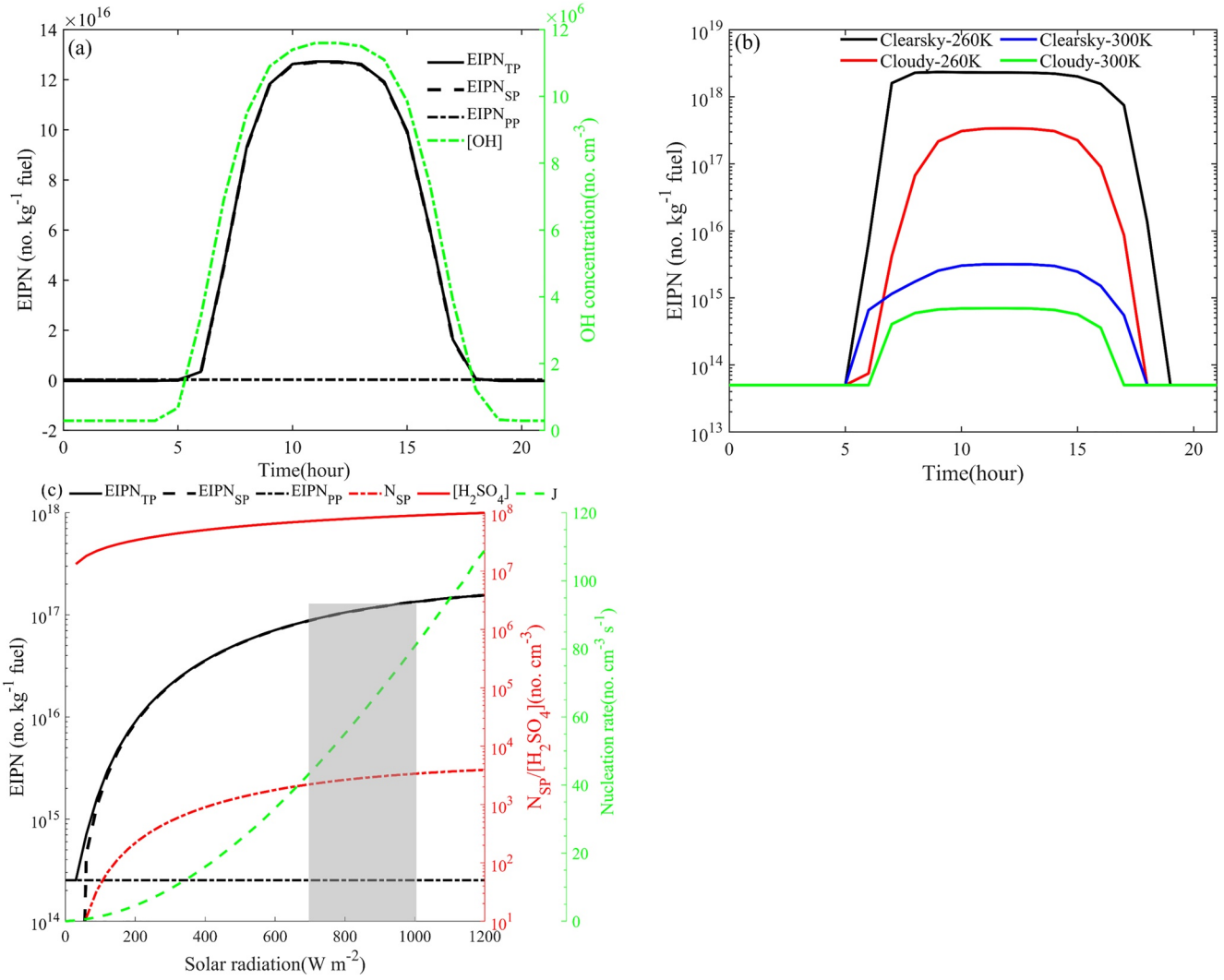

Figure 5. Sensitivity of emission index of particle number to photolysis. (a) Emission index of total, secondary, and primary particle numbers ($EIPN_{TP}$, $EIPN_{SP}$, $EIPN_{PP}$), two-hour averaged [OH] radical on ship exhausts release time varying from 00:00 to 21:00; (b) $EIPN_{SP}$ under clear sky and cloudy sky conditions and at different temperatures (260 and 300 K); (c) $EIPN_{TP}$, $EIPN_{SP}$, $EIPN_{PP}$, N_{SP}, two-hour averaged nucleation rate (J), and two-hour averaged [H_2SO_4] as a function of solar irradiation. The range of solar radiation measured during the ITCT 2K2 experiment is shaded in gray.

sitive to *T* when *T* changes from 250–270 K and 280–300 K, a 10 K difference in *T* can cause up to around 1 order of magnitude change in the N_{SP} and $EIPN_{SP}$. The nonlinear relationship is mainly caused by the dominance of different nucleation processes (homogeneous vs. ion-mediated nucleation). The dependence of EIPN on temperature is similar to that of nucleation rate (J) on temperature in Yu, Nadykto, et al. (2018). New particle formation may be suppressed by the effects of global warming, causing a reduction of the particle number in ship plumes, a subsequent CCN abundance and aerosol indirect radiative cooling, which requires further study. It should be noted that sea spray emissions also depend on sea surface temperature (Jaeglé et al., 2011). As shown in Section 4.1, sea salt emissions can indirectly affect particle formation in ship plumes. The effect of sea surface temperature change on sea salt emission and hence particle formation in ship plumes remains to be studied.

4.4. SO_2 Emission Rates and Background Concentration of SO_2

The SO_2 level in the plume is determined by the SO_2 emission rates and background SO_2 in addition to the dilution process. Figure 7a displays the influence of the SO_2 emission rates on $EIPN_{TP}$, $EIPN_{SP}$, $EIPN_{PP}$,

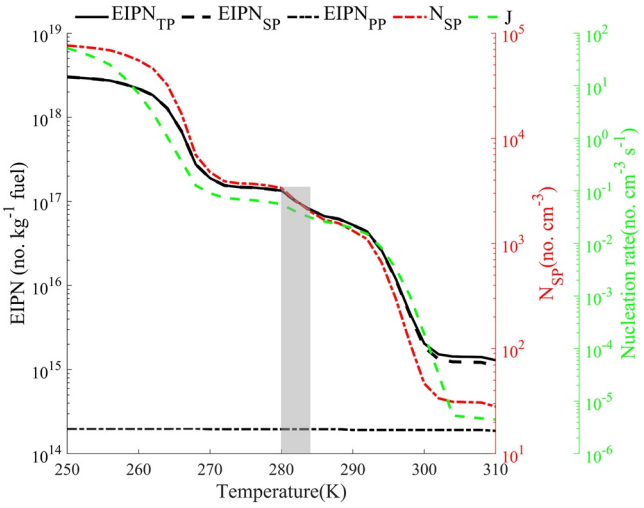

Figure 6. Dependence of $EIPN_{TP}$, $EIPN_{SP}$, $EIPN_{PP}$, two-hour averaged nucleation rate (J), and N_{SP} on temperature (T). The range of temperature measured during the ITCT 2K2 experiment is shaded in gray.

two-hour averaged H_2SO_4 concentrations, two-hour averaged nucleation rate (J), and N_{SP}. As pointed out earlier, $EIPN_{TN}$ is dominated by $EIPN_{SP}$. Higher SO_2 emission rates increase gaseous H_2SO_4, leading to higher levels of N_{SP} and $EIPN_{SP}$. $EIPN_{SP}$ ranges from 6.72×10^{15} to 3.83×10^{17} no. kg^{-1} fuel and is sensitive to the SO_2 emission rates when they are under 30 g s^{-1}. Since 2011, Emission Control Areas (ECAs) were gradually built in Europe, America, and China. Recently, according to the International Maritime Organization (IMO) regulation (UNCTAD, 2019), the maximum fuel sulfur content (FSC) has been lowered from 3.5% to 0.5% globally for ocean-going vessels from 2020; this value is even more stringently limited to 0.1% within 200 nautical miles of the Baltic Sea, the North Sea, North American emission control area, and the Caribbean Sea (Feng et al., 2019; Viana et al., 2015). Practically, the global mean sulfur content is about 2.6% in 2019 (IMO, 2020). Since the emission rate is not only determined by the sulfur content changes but also the combustion efficiency and engine power conditions, we take the emission rate of 9.38 g s^{-1} in ITCT 2K2 (2.2% FSC, 67% engine loading factor) to scale the emission rates under the variable sulfur contents of 3.5%, 2.6%, 0.5% and 0.1%. Under the conditions specified for Figure 7, the EIPN changes by a factor of ~5–7 with FSC decreasing from 2.6% and 3.5% to 0.5%. When the FSC is stringently limited, the EIPN changes by a factor of ~11 and 15 with the FSC decreasing from 2.6% and 3.5% to 0.1%. Sulfate aerosols may decrease with the wider application of lower FSC. The resulting decrease may be unfavorable for global warming mitigation, since Rasch et al. (2008) revealed that sulfate aerosols can counteract the global warming associated with increasing greenhouse gases and reduce changes to some other components of the Earth system. Compared with that of the SO_2 emission rate, the effect of the background SO_2 concentration on $EIPN_{SP}$ is weaker (Figure 7b). With the background concentration of SO_2 increasing from 0 to 3 ppbv, the gaseous H_2SO_4 concentrations and nucleation rates increased, which caused the N_{SP} and $EIPN_{SP}$ to increase by approximately one order of magnitude, from 9.91×10^2 to 9.78×10^3 no. cm^{-3} and 3.96×10^{16} to 3.88×10^{17} no. kg^{-1} fuel, respectively. It should be noted that $EIPN_{SP}$ is not sensitive to background SO_2 when its value is > 3 ppbv.

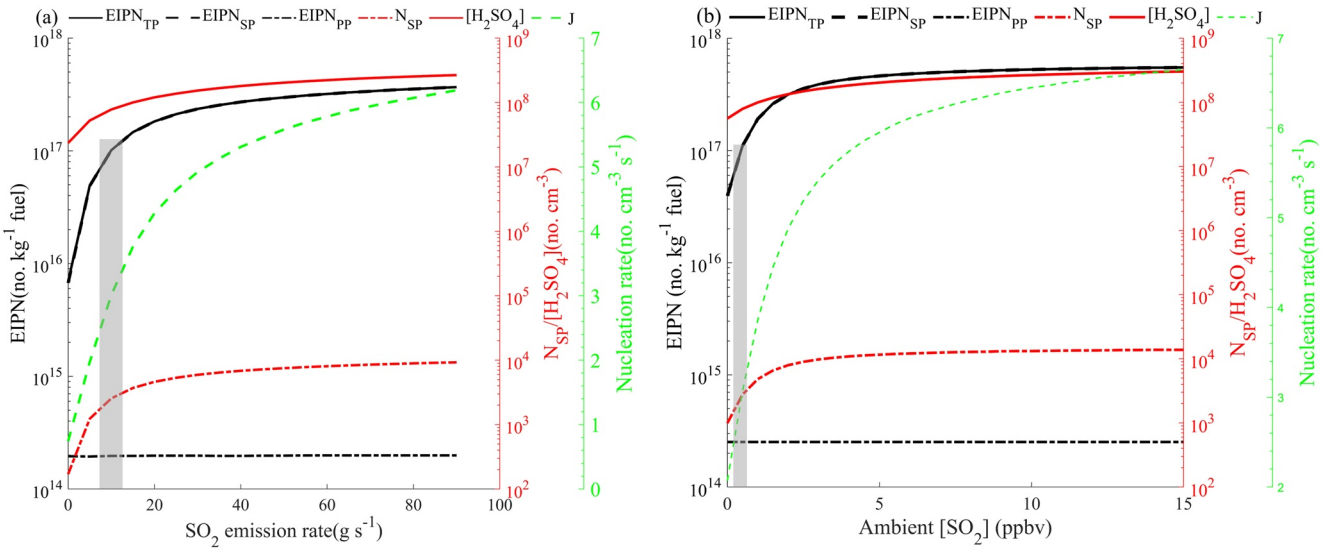

Figure 7. (a) Emission index of total, secondary, and primary particle numbers ($EIPN_{TP}$, $EIPN_{SP}$, $EIPN_{PP}$), two-hour averaged [H_2SO_4], N_{SP} ($[PN_{tot}] - [PN_{bg}]$), and two-hour averaged nucleation rate (J) as a function of emission rate of SO_2; (b) same as (a) but as a function of ambient SO_2 concentrations. The range of observed values during the ITCT 2K2 experiment is shaded in gray.

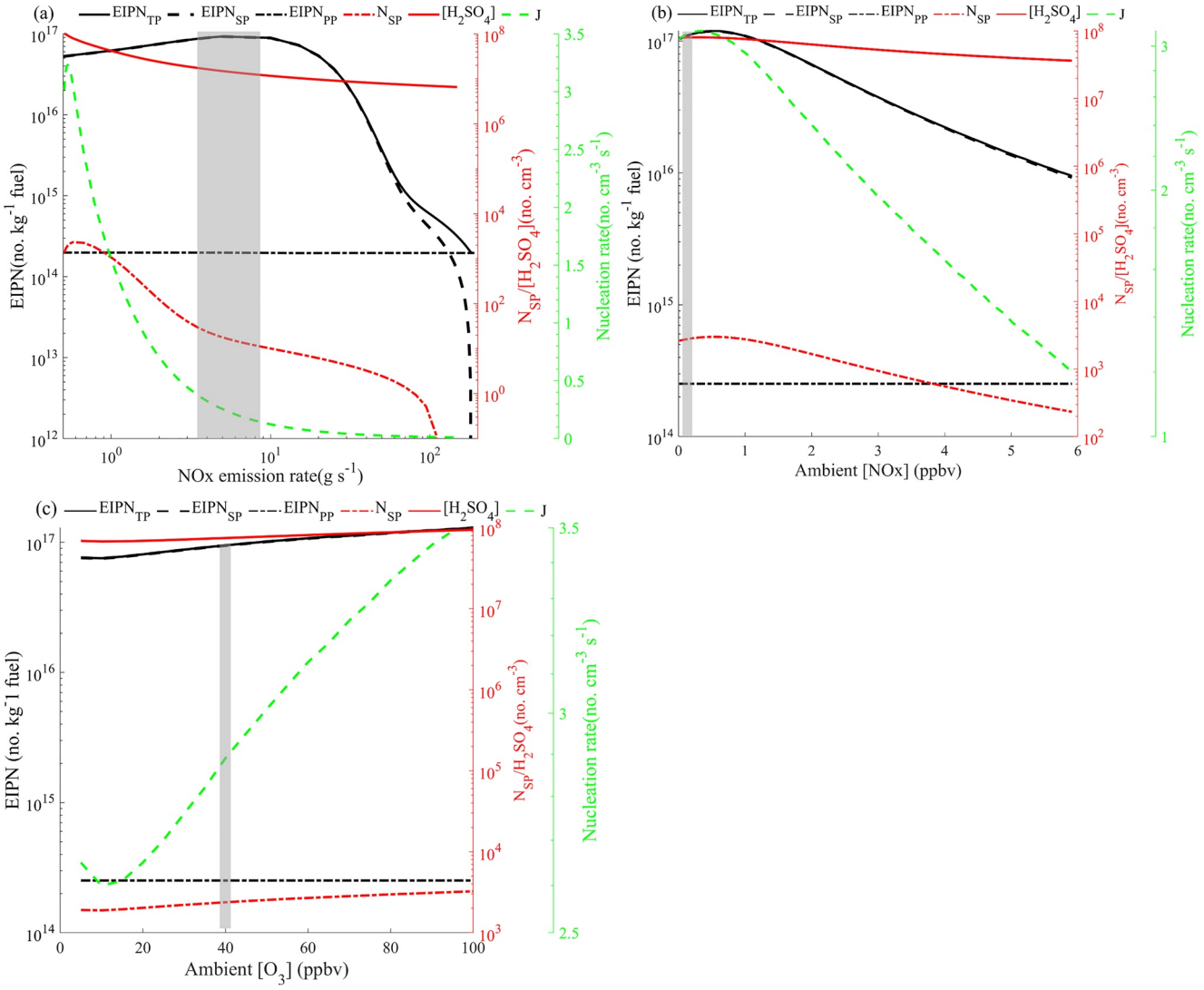

Figure 8. Sensitivity of emission index of particle number to NO_x emission rates and background concentration of NO_x, and O_3. (a) Dependence of $EIPN_{TP}$, $EIPN_{SP}$, $EIPN_{PP}$, two-hour averaged $[H_2SO_4]$, two-hour averaged nucleation rate (J), and N_{SP} on NO_x emission rates; (b) same as (a) but for a function of ambient $[NO_x]$; (c) same as (a) but for a function of ambient $[O_3]$. The area shaded in gray in (a–c) is the range of NO_x emission rates, ambient $[NO_x]$, and ambient $[O_3]$, respectively, observed during the ITCT 2K2 experiment.

4.5. NO_x Emission Rates and Background Concentrations of NO_x and O_3

Figure 8a shows the dependence of $EIPN_{TP}$, $EIPN_{SP}$, $EIPN_{PP}$, two-hour averaged concentration of H_2SO_4, two-hour averaged nucleation rate, and N_{SP} on the NO_x emission rates. Primary particles dominate in the plume when the NO_x emission rate is above 140 g s^{-1}. The NO_x emission rates have a significant impact on $EIPN_{SP}$, which increases from 4.66×10^{12} to 9.27×10^{16} no. kg^{-1} fuel as the NO_x emission rate changes from 5 to 180 g s^{-1}, and there is a slight increase when NO_x emission rates change from 0.5 to 5 g s^{-1} with EIPN ranging from 5.26×10^{16} to 9.27×10^{16} no. kg^{-1} fuel. $EIPN_{SP}$ decreased rapidly as the NO_x emission rates (>5 g s^{-1}) increased. It should be emphasized that OH radical is a key species in generating H_2SO_4. High NO_x emission rates lead to high NO levels, which reduce O_3 levels via NO and O_3 reaction and reduce OH production via photolysis reaction of O_3. It can be seen that the sensitivity of $EIPN_{SP}$ at a low NO_x emission rate (5–65 g s^{-1}) is greater than that at a relatively high NO_x emission rate (70–150 g s^{-1}), which is likely caused by the higher NO level decelerating the production of OH radicals. Such as, when the NO_x emission rate increases from 5 to 40 g s^{-1}, the H_2SO_4 level decreases from 7.88×10^7 to 2.72×10^7 no. cm^{-3}, which causes the nucleation rate to decrease to 1 no. cm^{-3} s^{-1} and the N_{SP} and $EIPN_{SP}$ to decrease by approximately 1 or-

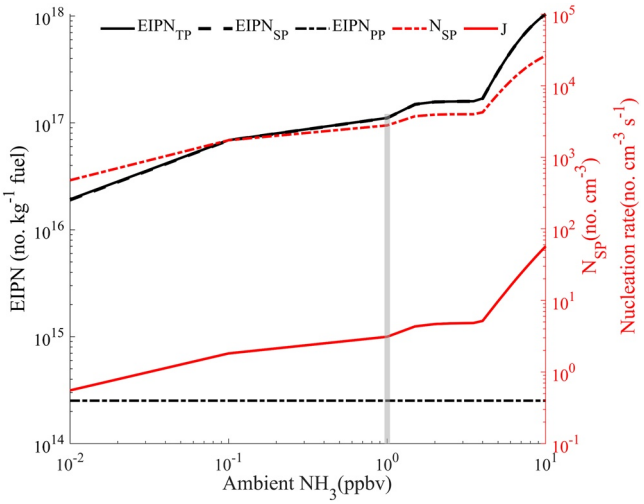

Figure 9. Dependence of $EIPN_{TP}$, $EIPN_{SP}$, $EIPN_{PP}$, two-hour averaged nucleation rate (J), and N_{SP} on ambient NH_3 concentrations. The range of $[NH_3]$ observed during the ITCT 2K2 experiment is shaded in gray.

der of magnitude. There is a NO_x emission control region around Europe (Karl et al., 2019) and our study indicate that such a control may slightly decrease the formation of new particles in ship plumes. Figures 8b and 8c give $EIPN_{TP}$, $EIPN_{SP}$, $EIPN_{PP}$, two-hour averaged concentration of H_2SO_4, two-hour averaged nucleation rate (J), and N_{SP} as a function of ambient $[NO_x]$ and $[O_3]$, respectively. Neither the changes of ambient $[NO_x]$ nor $[O_3]$ dramatically affect $[H_2SO_4]$ and thus fail to change the nucleation rate and new particle formation (N_{SP}). Hence, $EIPN_{SP}$ decreased slightly from 1.20×10^{17} to 9.44×10^{16} no. kg^{-1} fuel, with the background concentration of NO_x increasing from 10 pptv to 6 ppbv (Figure 8b). Similarly, $EIPN_{SP}$ is slightly changed, with the background concentration of O_3 increasing, from 7.59×10^{16} to 1.29×10^{17} no. kg^{-1} fuel (Figure 8c), although there was an obvious impact on the remaining NO_x and integrated net ozone production efficiency in the ship plume (Vinken et al., 2011). In total, the NO_x emission rate has a strong impact on $EIPN_{SP}$, with an approximate change of 4 orders of magnitude, while $EIPN_{SP}$ is insensitive to background concentrations of $[NO_x]$ and $[O_3]$.

4.6. The Background Concentration of NH_3

As a key parameter of new particle formation, NH_3, directly affecting the nucleation rate, is investigated in the sensitivity to emission index of particle numbers. Figure 9 shows the dependence of $EIPN_{TP}$, $EIPN_{SP}$, $EIPN_{PP}$, two-hour averaged nucleation rate, and N_{SP} on the concentration of ambient ammonia ($[NH_3]$), with other parameters the same as the baseline case. $EIPN_{SP}$ changed 1 order of magnitude (1.07×10^{16} to 1.11×10^{17} no. kg^{-1} fuel) when $[NH_3]$ increased from 0.01 to 1 ppbv. The simulations include a "zero-sensitivity zone" in the region of 2–4 ppbv of $[NH_3]$ ($\sim 1.7 \times 10^{17}$ no. kg^{-1} fuel) (caused by the limitation of nucleation rate by the ionization rate, Yu, Nadykto, et al., 2018), followed by a region of strong sensitivity of $EIPN_{SP}$, increasing from 2.31×10^{17} to 1.08×10^{18} no. kg^{-1} fuel to $[NH_3]$ commencing at $[NH_3] > 4$–10 ppbv as the nucleation rate rapidly increases. The latter zone may have important implications for nucleation process in heavily polluted coastal regions, including India and China, where $[NH_3]$ may exceed 5 ppbv (Kumar et al., 2016; S. Wang et al., 2015).

5. Conclusions and Discussions

In the present work, we integrated a photochemistry box model (BOXMOX) with a size-resolved particle microphysics model (APM) and applied the model to investigate key controlling parameters on the particle number emission index. Comparisons of simulated concentrations of SO_2, NO_x, O_3, H_2SO_4, and the total particle number with measurements from ITCT 2K2 taken off the California coast show good agreement, indicating that the model is able to capture key chemistry and particle microphysics in ship plumes. We show that significant formation of new particles via ternary ion-mediated nucleation occurs shortly after emission of exhaust and these secondary particles generally dominate the total particle number concentrations.

Our systematic model simulations indicate that combined wind speed and sea salt concentration, SO_2 emission rate, NO_x emission rate, solar irradiation, ambient temperature, and background $[NH_3]$ can all affect the emission index of secondary particle numbers, resulting in a large range of secondary particle number emission index with the values in the range of 1.0×10^{14}–1.01×10^{17}, 6.72×10^{15}–3.83×10^{17}, 4.66×10^{12}–9.27×10^{16}, 1.0×10^{14}–1.56×10^{17}, 1.23×10^{15}–3.81×10^{18}, and 1.07×10^{16}–1.08×10^{18} no. kg-$fuel^{-1}$, respectively. The results highlight the sensitivity of new particle formation during the evolution of ship plumes to emission rates of precursors and ambient conditions. Specifically, ship emissions may imply important feedback to the climate with expected increased shipping through the Arctic since low temperature can facilitate new particle formation. Moreover, we demonstrate that the lowering of the FSC from a typical value of 3.5% or 2.6% globally to 0.5% is expected to decrease $EIPN_{SP}$ linearly, but with its further reduction to 0.1%, the reduction in $EIPN_{SP}$ would be nonlinear.

We must note that due to limited field measurements, only the NOAA ITCT 2K2 experimental data was employable to validate model simulations in this study. Hopefully, the findings in this study could help urge comprehensive measurements and deepen the research field in the near future. Moreover, future work will focus on developing parameterizations of key gaseous species and particle number emission factors under various environmental conditions including wind speed, emission rates of SO_2 and NO_x, solar irradiation, ambient temperature, and background [NH_3] for 3-D modeling applications, and generating lookup tables for parameterizing subgrid ship particle number emissions to study the impact of shipping emissions on the marine aerosol number abundance, CCN, and climate after understanding key parameters that control particle formation in ship plumes. The BOXMOX-APM can also be applied to study chemistry and particle microphysics in other plumes, such as those from motor vehicles, power plants, and aircrafts, as well as heterogeneous chemistry.

Conflict of Interest

The authors declare no conflicts of interest relevant to this study.

Data Availability Statement

All the ITCT 2K2 airborne data sets can be obtained from the official NOAA data archive at https://esrl.noaa.gov/csl/groups/csl7/measurements/2002ITCT/P3/DataDownload. (last access: 5 November 2020).

Acknowledgments
This work was supported by the National Natural Science Foundation of China (42077195), the Key-Area Research and Development Program of Guangdong Province (2020B1111360001), the National Key Research and Development Program of China (2016YFA060130X), and the National Science Foundation of USA (AGS-1550816). The authors thank the BOXMOX developers for making the model available for the community to use.

References

Agrawal, H., Malloy, Q. G. J., Welch, W. A., Miller, J. W., & Cocker, D. R. (2008). In-use gaseous and particulate matter emissions from a modern oceangoing container vessel. *Atmospheric Environment*, *42*, 5504–5510. https://doi.org/10.1016/j.atmosenv.2008.02.053

Alicke, B., Geyer, A., Hofzumahaus, A., Holland, F., Konrad, S., Patz, H. W., et al. (2003). OH formation by HONO photolysis during the BERLIOZ experiment. *Journal of Geophysical Research*, *108*(D4), 8247. https://doi.org/10.1029/2001JD000579

Arnold, S. R., Spracklen, D. V., Williams, J., Yassaa, N., Sciare, J., Bonsang, B., et al. (2009). Evaluation of the global oceanic isoprene source and its impacts on marine organic carbon aerosol. *Atmospheric Chemistry and Physics*, *9*(4), 1253–1262. https://doi.org/10.5194/acp-9-1253-2009

Brock, C. A., Hudson, P. K., Lovejoy, E. R., Sullivan, A., Nowak, J. B., Huey, L. G., et al. (2004). Particle characteristics following cloud-modified transport from Asia to North America. *Journal of Geophysical Research*, *109*, D23S26. https://doi.org/10.1029/2003JD004198

Calvert, J. G., Yarwood, G., & Dunker, A. M. (1994). An evaluation of the mechanism of nitrous acid formation in the urban atmosphere. *Research on Chemical Intermediates*, *20*(3–5), 463–502. https://doi.org/10.1163/156856794X00423

Cao, Y., Zhang, W., Wang, X., Wu, L., & Qian, G. (2019). The relationship between atmospheric pollutant emissions and fuel qualities of inland vessels in Jiangsu Province, China. *Journal of the Air & Waste Management Association*, *69*(3), 305–312. https://doi.org/10.1080/10962247.2018.1531796

Capaldo, K., Corbett, J. J., Kasibhatla, P., Fischbeck, P., & Pandis, S. N. (1999). Effects of ship emissions on sulphur cycling and radiative climate forcing over the ocean. *Nature*, *400*, 743–746. https://doi.org/10.1038/23438

Capaldo, K., Kasibhatla, P., & Pandis, S. N. (1999). Is aerosol production within the remote marine boundary layer sufficient to maintain observed concentrations? *Journal of Geophysical Research*, *104*, 3483–3500. https://doi.org/10.1029/1998JD100080

Chen, G., Huey, L. G., Trainer, M., Nicks, D., Corbett, J., Ryerson, T., et al. (2005). An investigation of the chemistry of ship emission plumes during ITCT 2002. *Journal of Geophysical Research*, *110*, D10S90. https://doi.org/10.1029/2004JD005236

Christensen, M. W., & Stephens, G. L. (2012). Microphysical and macrophysical responses of marine stratocumulus polluted by underlying ships: 2. Impacts of haze on precipitating clouds. *Journal of Geophysical Research*, *117*, D11203. https://doi.org/10.1029/2011JD017125

Christensen, M. W., Suzuki, K., Zambri, B., & Stephens, G. L. (2015). Ship track observations of a reduced shortwave aerosol indirect effect in mixed-phase clouds. *Geophysical Research Letters*, *41*(19), 6970–6977. https://doi.org/10.1002/2014GL061320

Cohen, A. J., Anderson, H. R., Ostro, B., Pandey, K. D., Krzyzanowski, M., Kunzli, N., et al. (2005). The global burden of disease due to outdoor air pollution. *Journal of Toxicology and Environmental Health, Part A*, *68*, 1301–1307. https://doi.org/10.1080/15287390590936166

Cooper, D. A., & Gustafsson, T. (2004). *Methodology for calculating emissions from ships: 1. Update of emission factors*. (Report Series SMED and SMED&SLU 4). (p. 45). Norrköping: Swedish Meteorological and Hydrological Institute.

Diamond, M. S., Director, H. M., Eastman, R., Possner, A., & Wood, R. (2020). Substantial cloud brightening from shipping in subtropical low clouds. *AGU Advances*, *1*, e2019AV000111. https://doi.org/10.1029/2019AV000111

Diesch, J.-M., Drewnick, F., Klimach, T., & Borrmann, S. (2013). Investigation of gaseous and particulate emissions from various marine vessel types measured on the banks of the Elbe in Northern Germany. *Atmospheric Chemistry and Physics*, *13*, 3603–3618. https://doi.org/10.5194/acp-13-3603-2013

Dominguez, G., Jackson, T., Brothers, L., Barnett, B., Nguyen, B., & Thiemens, M. H. (2008). Discovery and measurement of an isotopically distinct source of sulfate in Earth's atmosphere. *Proceedings of the National Academy of Sciences*, *105*(35), 12769–12773. https://doi.org/10.1073/pnas.0805255105

Durkee, P., Noone, K., & Bluth, R. (2000). The Monterey area ship track experiment. *Journal of the Atmospheric Sciences*, *57*, 2523–2541. https://doi.org/10.1175/1520-0469(2000)057<2523:TMASTE>2.0.CO;2

Emmons, L., Walters, S., Hess, P., Lamarque, J. F., Pfister, G., Fillmore, D., et al. (2010). Description and evaluation of the model for ozone and related chemical tracers, version 4 (MOZART-4). *Geoscientific Model Development*, *3*(1), 43–67. https://doi.org/10.5194/gmd-3-43-2010

Endresen, Ø., Sørgard, E., Sundet, J. K., Dalsøren, S. B., Isaksen, I. S. A., Berglen, T. F., et al. (2003). Emission from international sea transportation and environmental impact. *Journal of Geophysical Research*, *108*(D17), 4560. https://doi.org/10.1029/2002JD002898

EPA (2000). *Analysis of commercial marine vessels emissions and fuel consumption data*. (Tech. Rep. EPA420-R-00-002). United States Environmental Protection Agency. https://nepis.epa.gov/Exe/ZyPDF.cgi/P1009Z2K.PDF?Dockey=P1009Z2K.PDF

Eyring, V., Isaksen, I. S. A., Berntsen, T., Collins, W. J., Corbett, J. J., Endresen, O., et al. (2010). Transport impacts on atmosphere and climate: Shipping. *Atmospheric Environment*, *44*, 4735–4771. https://doi.org/10.1016/j.atmosenv.2009.04.059

Fagerlund, A. J., Iversen, M., Ekeland, A., Moen, C. M., & Aslaksen, P. M. (2019). Blame it on the weather? The association between pain in fibromyalgia, relative humidity, temperature and barometric pressure. *PLoS ONE*, *14*(5), e0216902. https://doi.org/10.1371/journal.pone.0216902

Feng, J., Zhang, Y., Li, S., Mao, J., Patton, A. P., Zhou, Y., et al. (2019). The influence of spatiality on shipping emissions, air quality and potential human exposure in the Yangtze River Delta/Shanghai, China. *Atmospheric Chemistry and Physics*, *19*, 6167–6183. https://doi.org/10.5194/acp-19-6167-2019

Fitzgerald, J. W. (1973). Dependence of the supersaturation spectrum of CCN on aerosol size distribution and composition. *Journal of the Atmospheric Sciences*, *30*, 628–634. https://doi.org/10.1175/1520-0469(1973)030<0628:DOTSSO>2.0.CO;2

Frick, G. M., & Hoppel, W. A. (2000). Airship measurements of Ship's exhaust plumes and their effect on marine boundary layer clouds. *Journal of the Atmospheric Sciences*, *57*, 2625–2648. https://doi.org/10.1175/1520-0469(2000)057<2625:AMOSSE>2.0.CO;2

Gantt, B., Meskhidze, N., Zhang, Y., & Xu, J. (2010). The effect of marine isoprene emissions on secondary organic aerosol and ozone formation in the coastal United States. *Atmospheric Environment*, *44*(1), 115–121. https://doi.org/10.1016/j.atmosenv.2009.08.027

Gong, S. L., Barrie, L. A., & Blanchet, J. P. (1997). Modeling sea-salt aerosols in the atmosphere: 1. Model development. *Journal of Geophysical Research: Atmospheres*, *102*(D3), 3805–3818. https://doi.org/10.1029/96JD02953

Griffin, R. J., Cocker, D. R., Seinfeld, J. H., & Dabdub, D. (1999). Estimate of global atmospheric organic aerosol from oxidation of biogenic hydrocarbons. *Geophysical Research Letters*, *26*(17), 2721–2724. https://doi.org/10.1029/1999GL900476

Hanna, S. R., Schulman, L. L., Paine, R. J., Pleim, J., & Baer, M. (1985). Development and evaluation of the offshore and coastal dispersion model. *Journal of the Air Pollution Control Association*, *35*, 1039–1047. https://doi.org/10.1080/00022470.1985.10466003

Hoffmann, T., Odum, J. R., Bowman, F., Collins, D., Klockow, D., Flagan, R. C., & Seinfeld, J. H. (1997). Formation of organic aerosols from the oxidation of biogenic hydrocarbons. *Journal of Atmospheric Chemistry*, *26*(2), 189–222. https://doi.org/10.1023/A:1005734301837

Hong, G., Yang, P., Gao, B.-C., Baum, B. A., Hu, Y. X., King, M. D., & Platnick, S. (2007). High cloud properties from three years of MODIS Terra and Aqua collection-4 data over the tropics. *Journal of Applied Meteorology and Climatology*, *46*, 1840–1856. https://doi.org/10.1175/2007JAMC1583.1

IMO. (2020). *Report of the maritime safety committee on its 75th session*. (MEPC 75/5/9). https://docs.imo.org/Documents/Detail.aspx?did=123561

Jacobson, M. Z., Wilkerson, J. T., Naiman, A. D., & Lele, S. K. (2011). The effects of aircraft on climate and pollution, Part I: Numerical methods for treating the subgrid evolution of discrete size- and composition-resolved contrails from all commercial flights worldwide. *Journal of Computational Physics*, *230*, 5115–5132. https://doi.org/10.1016/j.jcp.2011.03.031

Jaeglé, L., Quinn, P. K., Bates, T. S., Alexander, B., & Lin, J.-T. (2011). Global distribution of sea salt aerosols: New constraints from in situ and remote sensing observations. *Atmospheric Chemistry and Physics*, *11*, 3137–3157. https://doi.org/10.5194/acp-11-3137-2011

Jonsson, Å. M., Westerlund, J., & Hallquist, M. (2011). Size-resolved particle emission factors for individual ships. *Geophysical Research Letters*, *38*, L13809. https://doi.org/10.1029/2011GL047672

Junge, C., & McLaren, E. (1971). Relationship of cloud nuclei spectra to aerosol size distribution and composition. *Journal of the Atmospheric Sciences*, *28*, 382–390. https://doi.org/10.1175/1520-0469(1971)028<0382:ROCNST>2.0.CO;2

Juwono, A. M., Johnson, G. R., Mazaheri, M., Morawska, L., Roux, F., & Kitchen, B. (2013). Investigation of the airborne submicrometer particles emitted by dredging vessels using a plume capture method. *Atmospheric Environment*, *73*, 112–123. https://doi.org/10.1016/j.atmosenv.2013.03.024

Karl, M., Bieser, J., Geyer, B., Matthias, V., Jalkanen, J.-P., Johansson, L., & Fridell, E. (2019). Impact of a nitrogen emission control area (NECA) on the future air quality and nitrogen deposition to seawater in the Baltic Sea region. *Atmospheric Chemistry and Physics*, *19*, 1721–1752. https://doi.org/10.5194/acp-19-1721-2019

Kim, H. S., Song, C. H., Park, R. S., Huey, G., & Ryu, J. Y. (2009). Investigation of ship-plume chemistry using a newly-developed photochemical/dynamic ship-plume model. *Atmospheric Chemistry and Physics*, *9*, 7531–7550. https://doi.org/10.5194/acp-9-7531-2009

Kirkby, J., Curtius, J., Almeida, J., Dunne, E., Duplissy, J., Ehrhart, S., et al. (2011). The role of sulfuric acid, ammonia and galactic cosmic rays in atmospheric aerosol nucleation. *Nature*, *476*, 429–433. https://doi.org/10.1038/nature10343

Knote, C., Tuccella, P., Curci, G., Emmons, L., Orlando, J. J., Madronich, S., et al. (2015). Influence of the choice of gas-phase mechanism on predictions of key gaseous pollutants during the AQMEII phase-2 intercomparison. *Atmospheric Environment*, *115*, 553–568. https://doi.org/10.1016/j.atmosenv.2014.11.066

Kuang, C., McMurry, P. H., McCormick, A. V., & Eisele, F. L. (2008). Dependence of nucleation rates on sulfuric acid vapor concentration in diverse atmospheric locations. *Journal of Geophysical Research: Atmospheres*, *113*, D10209. https://doi.org/10.1029/2007JD009253

Kulmala, M., & Laaksonen, A. (1990). Binary nucleation of water sulfuric acid system: Comparison of classical theories with different H_2SO_4 saturation vapor pressures. *Journal of Chemical Physics*, *93*, 696–701. https://doi.org/10.1063/1.459519

Kumar, A., Gupta, I., Brandt, J., Kumar, R., Dikshit, A. K., & Patil, R. S. (2016). Air quality mapping using GIS and economic evaluation of health impact for Mumbai City, India. *Journal of Air Waste Management Association*, *66*, 470–481. https://doi.org/10.1080/10962247.2016.1143887

Lack, D. A., Cappa, C. D., Langridge, J., Bahreini, R., Buffaloe, G., Brock, C., et al. (2011). Impact of fuel quality regulation and speed reductions on shipping emissions: Implications for climate and air quality. *Environmental Science & Technology*, *45*, 9052–9060. https://doi.org/10.1021/es2013424

Lack, D. A., Corbett, J. J., Onasch, T., Lerner, B., Massoli, P., Quinn, P. K., et al. (2009). Particulate emissions from commercial shipping: Chemical, physical, and optical properties. *Journal of Geophysical Research*, *114*, D00F04. https://doi.org/10.1029/2008JD011300

Lawrence, M. G., & Crutzen, P. J. (1999). Influence of NO_x emissions from ships on tropospheric photochemistry and climate. *Nature*, *402*, 167–170. https://doi.org/10.1038/46013

Luo, G., & Yu, F. (2011). Simulation of particle formation and number concentration over the Eastern United States with the WRF-Chem + APM model. *Atmospheric Chemistry and Physics*, *11*, 11521–11533. https://doi.org/10.5194/acp-11-11521-2011

Neitola, K., Brus, D., Makkonen, U., Sipilä, M., Mauldin, R. L., III, Sarnela, N., et al. (2015). Total sulfate vs. sulfuric acid monomer concentrations in nucleation studies. *Atmospheric Chemistry and Physics*, *15*, 3429–3443. https://doi.org/10.5194/acp-15-3429-2015

Nowak, J. B., Parrish, D. D., Neuman, J. A., Holloway, J. S., Cooper, O. R., Ryerson, T. B., et al. (2004). Gas-phase chemical characteristics of Asian emission plumes observed during ITCT 2K2 over the eastern North Pacific Ocean. *Journal of Geophysical Research*, *109*, D23S19. https://doi.org/10.1029/2003JD004488

O'Dowd, C. D., McFiggans, G., Creasey, D. J., Pirjola, L., Hoell, C., Smith, M. H., et al. (1999). On the photochemical production of new particles in the coastal boundary layer. *Geophysical Research Letters*, *26*, 1707–1710. https://doi.org/10.1029/1999GL900335

Palancar, G. G., Fernández, R. P., & Toselli, B. M. (2005). Photolysis rate coefficients calculations from broadband UV-B irradiance: Model-measurement interaction. *Atmospheric Environment*, *39*, 857–866. https://doi.org/10.1016/j.atmosenv.2004.10.033

Parrish, D. D., Kondo, Y., Cooper, O. R., Brock, C. A., Jaffe, D. A., Trainer, M., et al. (2004). Intercontinental transport and chemical transformation 2002 (ITCT 2K2) and Pacific Exploration of Asian Continental Emission (PEACE) experiments: An overview of the 2002 winter and spring intensives. *Journal of Geophysical Research*, *109*, D23S01. https://doi.org/10.1029/2004JD004980

Quinn, P., Charlson, R., & Zoller, W. (1987). Ammonia, the dominant base in the remote marine troposphere: A review. *Tellus B: Chemical and Physical Meteorology*, *39*(5), 413–425. https://doi.org/10.3402/tellusb.v39i5.15359

Ramana, M. V., & Devi, A. (2016). CCN concentrations and BC warming influenced by maritime ship emitted aerosol plumes over southern Bay of Bengal. *Scientific Reports*, *6*(30416), 1–8. https://doi.org/10.1038/srep30416

Rasch, P. J., Tilmes, S., Turco, R. P., Robock, A., Oman, L., Chen, C.-C. J., et al. (2008). An overview of geoengineering of climate using stratospheric sulphate aerosols. *Philosophical Transactions of the Royal Society A*, *366*(1882), 4007–4037. https://doi.org/10.1098/rsta.2008.0131

Russell, L., Seinfeld, J., Flagan, R., Ferek, R., Hegg, D., Hobbs, P., et al. (1999). Aerosol dynamics in ship tracks. *Journal of Geophysical Research*, *104*, 31077–31095. https://doi.org/10.1029/1999JD900985

Sinha, P., Hobbs, P. V., Yokelson, R. J., Christian, T. J., Kirchstetter, T. W., & Bruintjes, R. (2003). Emissions of trace gases and particles from two ships in the southern Atlantic Ocean. *Atmospheric Environment*, *37*, 2139–2148. https://doi.org/10.1016/S1352-2310(03)00080-3

Song, C. H., Chen, G., & Davis, D. D. (2003). Chemical evolution and dispersion of ship plumes in the remote marine boundary layer: Investigation of sulfur chemistry. *Atmospheric Environment*, *37*, 2663–2679. https://doi.org/10.1016/S1352-2310(03)00198-5

Song, C. H., Chen, G., Hanna, S. R., Crawford, J., & Davis, D. D. (2003). Dispersion and chemical evolution of ship plumes in the marine boundary layer: Investigation of $O_3/NO_y/HO_x$ chemistry. *Journal of Geophysical Research*, *108*(D4), 4143. https://doi.org/10.1029/2002JD002216

Song, C. H., Kim, H. S., von Glasow, R., Brimblecombe, P., Kim, J., Park, R. J., et al. (2010). Source identification and budget analysis on elevated levels of formaldehyde within the ship plumes: A ship-plume photochemical/dynamic model analysis. *Atmospheric Chemistry and Physics*, *10*, 11969–11985. https://doi.org/10.5194/acp-10-11969-2010

Thornton, J. A., Virts, K. S., Holzworth, R. H., & Mitchell, T. P. (2017). Lightning enhancement over major oceanic shipping lanes. *Geophysical Research Letters*, *44*(17), 9102–9111. https://doi.org/10.1002/2017GL074982

Tian, J., Riemer, N., West, M., Pfaffenberger, L., Schlager, H., & Petzold, A. (2014). Modeling the evolution of aerosol particles in a ship plume using PartMC-MOSAIC. *Atmospheric Chemistry and Physics*, *14*, 5327–5347. https://doi.org/10.5194/acp-14-5327-2014

Trebs, I., Bohn, B., Ammann, C., Rummel, U., Blumthaler, M., Königstedt, R., et al. (2009). Relationship between the NO_2 photolysis frequency and the solar global irradiance. *Atmospheric Measurement Techniques*, *2*, 725–739. https://doi.org/10.5194/amt-2-725-2009

Turco, R. P., Hamill, P., Toon, O. B., Whitten, R. C., & Kiang, C. S. (1979). A one-dimensional model describing aerosol formation and evolution in the stratosphere, Part I, Physical processes and mathematical analogs. *Journal of the Atmospheric Sciences*, *36*, 699–717. https://doi.org/10.1175/1520-0469(1979)036<0699:AODMDA>2.0.CO;2

UNCTAD. (2019). *Review of maritime transport 2019*. USA: UNITED NATIONS PUBLICATION. https://unctad.org/system/files/official-document/rmt2019_en.pdf

Viana, M., Fann, N., Tobías, A., Querol, X., Rojas-Rueda, D., Plaza, A., et al. (2015). Environmental and health benefits from designating the Marmara Sea and the Turkish Straits as an Emission Control Area (ECA). *Environmental Science & Technology*, *49*, 3304–3313. https://doi.org/10.1021/es5049946

Villa, T. F., Brown, R. A., Jayaratne, E. R., Gonzalez, L. F., Morawska&Ristovski, L. Z., & Ristovski, Z. D. (2019). Characterization of the particle emission from a ship operating at sea using an unmanned aerial vehicle. *Atmospheric Measurement Techniques*, *12*, 691–702. https://doi.org/10.5194/amt-12-691-2019

Vinken, G. C. M., Boersma, K. F., Jacob, D. J., & Meijer, E. W. (2011). Accounting for non-linear chemistry of ship plumes in the GEOS-Chem global chemistry transport model. *Atmospheric Chemistry and Physics*, *11*, 11707–11722. https://doi.org/10.5194/acp-11-11707-2011

Wang, S., Nan, J., Shi, C., Fu, Q., Gao, S., Qang, D., et al. (2015). Atmospheric ammonia and its impacts on regional air quality over the megacity of Shanghai, China. *Scientific Reports*, *5*, 15842. https://doi.org/10.1038/srep15842

Wang, X., Shen, Y., Lin, Y., Pan, J., Zhang, Y., Louie, P. K. K., et al. (2019). Atmospheric pollution from ships and its impact on local air quality at a port site in Shanghai. *Atmospheric Chemistry and Physics*, *19*, 6315–6330. https://doi.org/10.5194/acp-19-6315-2019"

Westerlund, J., Hallquist, M., & Hallquist, Å. M. (2015). Characterization of fleet emissions from ships through multi-individual determination of size-resolved particle emissions in a coastal area. *Atmospheric Environment*, *112*, 159–166. https://doi.org/10.1016/j.atmosenv.2015.04.018

Yang, C., Meng, X., Chen, R., Cai, J., Zhao, Z., Wan, Y., & Kan, H. (2015). Long-term variations in the association between ambient temperature and daily cardiovascular mortality in Shanghai, China. *The Science of the Total Environment*, *538*, 524–530. https://doi.org/10.1016/j.scitotenv.2015.08.097

Yu, F. (1998). *A study of the formation and evolution of aerosols and contrails in aircraft wakes: Development, validation and application of an advanced particle microphysics (APM) model*. (Doctoral Dissertation). UCLA.

Yu, F. (2006). From molecular clusters to nanoparticles: Second-generation ion-mediated nucleation model. *Atmospheric Chemistry and Physics*, *6*, 5193–5211. https://doi.org/10.5194/acp-6-5193-2006

Yu, F. (2010). Diurnal and seasonal variations of Ultrafine particle formation in anthropogenic SO_2 Plumes. *Environmental Science & Technology*, *44*, 2011–2015. https://doi.org/10.1021/es903228a

Yu, F., & Luo, G. (2009). Simulation of particle size distribution with a global aerosol model: Contribution of nucleation to aerosol and CCN number concentrations. *Atmospheric Chemistry and Physics*, *9*, 7691–7710. https://doi.org/10.5194/acp-9-7691-2009

Yu, F., Nadykto, A. B., Herb, J., Luo, G., Nazarenko, K. M., & Uvarova, L. A. (2018). H_2SO_4–H_2O–NH_3 ternary ion-mediated nucleation (TIMN): Kinetic-based model and comparison with CLOUD measurements. *Atmospheric Chemistry and Physics*, *18*, 17451–17474. https://doi.org/10.5194/acp-18-17451-2018

Yu, F., Nadykto, A. B., Luo, G., & Herb, J. (2020). H_2SO_4–H_2O binary and H_2SO_4–H_2O–NH_3 ternary homogeneous and ion-mediated nucleation: Lookup tables version 1.0 for 3-D modeling application. *Geoscientific Model Development*, *13*, 2663–2670. https://doi.org/10.5194/gmd-13-2663-2020

Yu, F., Nair, A. A., & Luo, G. (2018). Long-term trend of gaseous ammonia over the United States: Modeling and comparison with observations. *Journal of Geophysical Research: Atmospheres*, *123*, 8315–8325. https://doi.org/10.1029/2018JD028412

Yu, F., & Turco, R. P. (1997). The role of ions in the formation and evolution of particles in aircraft plumes. *Geophysical Research Letters*, *24*, 1927–1930. https://doi.org/10.1029/97GL01822